

GALAXY MOTIONS IN THE BOOTES STRIP

I. D. Karachentsev^{1,2(*)}, V. E. Karachentseva^{3(**)}, O. G. Nasonova^{1(***)}

¹*Special Astrophysical Observatory of RAS, Nizhny Arkhyz, Russia*

²*Leibniz-Institut für Astrophysik, Potsdam, Germany*

³*Main Astronomical Observatory of NASU, Kyiv, Ukraine*

We explore the structure and kinematics of a dispersed filament of galaxies residing between the Local Void and the Virgo cluster. For such purpose, we consider a sample of 361 galaxies with radial velocities $V_{LG} < 2000 \text{ km s}^{-1}$ inside the sky area of $[RA = 13.0^h - 18.0^h \text{ and } Dec. = -5^\circ - +10^\circ]$. At present, 161 of them have individual distance estimates. The galaxy distribution on peculiar velocities along the strip exhibits the known Virgo-centric infall at $RA < 14^h$ and some signs of outflow from the Local Void at $RA > 17^h$. Majority of the Bootes strip galaxies (56%) belong to 13 groups and 11 pairs, with the most prominent group around NGC 5846. The Bootes strip groups reside within $[17 - 27]$ Mpc, being all farther from us than the Virgo cluster. The Bootes filament contains the total stellar mass of $2.7 \times 10^{12} M_\odot$ and the total virial mass of $9.07 \times 10^{13} M_\odot$, having the average density of dark matter to be $\Omega_m = 0.09$, i.e. a factor three lower than the global cosmic average.

Keywords: galaxies: distances and redshifts, (cosmology:) large-scale structure of Universe

1 Introduction

Recent mass measurements of radial velocities and distances of galaxies engage for obtaining shortly the detailed map of peculiar motions within the Local Supercluster. Since the peculiar velocities field is generated by the dark matter distribution in the considered volume and its neighbourhood, invoking N-body simulations to the analysis gives us a possibility to trace the large scale structure relief, i.e. the disposition of the main attractors and voids. According to Sorce et al. (2013), the constrained simulations method can spot some massive proximal attractors such as the Virgo cluster with an accuracy of about 5 Mpc.

However, as it was noticed by different authors (Venik 1984, Tully 1987, Makarov & Karachentsev 2011, Karachentsev 2012), the virial mass estimates of galaxy groups and clusters in the Local Universe lead to the average matter density value of $\Omega_m(local) \simeq 0.08$ which is 3 times lower than the global cosmological value $\Omega_m(global) = 0.24 \pm 0.03$ (Spergel et al. 2007). One of the possible explanations of this discrepancy is the assumption that the lacking 2/3 of the dark matter total amount are spread outside the virial radii of galaxy groups and clusters. Yet, the analysis of Hubble flows around the nearest aggregates: the Local Group (Karachentsev et al. 2009), M81 group (Karachentsev & Kashibadze 2006), Cen A group (Karachentsev et al. 2007), Virgo cluster

(Karachentsev & Nasonova 2010) and Fornax cluster (Nasonova et al. 2011) shows that the total masses of these groups and clusters within “zero velocity surface” radii, R_0 , are in a good agreement with the virial mass estimates, although R_0 radius is roughly 4 times larger than virial one. Hence, the major fraction of the lacking dark matter is spread outwith infall zones around groups and clusters. There are some suggestions in literature that significant amount of dark matter could be located in “dark filaments” conducting intergalactic matter into hot virial regions (Dietrich et al. 2012, Whitting 2006).

Obviously, the Local Supercluster is the most appropriate object to verify these hypotheses due to the high density of observational data on galaxy velocities and distances. In our previous papers we considered motions of galaxies in filaments attached to the Virgo cluster, as the centre of the Local Supercluster, from North and South. In Virgo Southern Extension region $[RA = 12.5^h - 13.5^h, Dec. = -20^\circ - 0^\circ]$ (Karachentsev & Nasonova 2013) and Ursa Majoris region $[RA = 11.0^h - 13.0^h, Dec. = +40^\circ - +60^\circ]$ (Karachentsev et al. 2013) the mean matter density was estimated to be $\Omega_m = 0.11$ and 0.08 , respectively. But we surmised the existence of a dark attractor with the mass of $\sim 2 \times 10^{14} M_\odot$ in the Coma I region $[RA = 11.5^h - 13.0^h, Dec. = +20^\circ - +40^\circ]$ (Karachentsev et al. 2011). All these three zones are situated along the equator of the Local Supercluster where the structure and kinematics of galaxy groups is some way faded away due to projection effects.

As it can be seen from the mapped distribution of

(*)E-mail: ikar@sao.ru

(**)E-mail: vakara@mao.kiev.ua

(***)E-mail: phiruzi@gmail.com

galaxies with radial velocities $V_{LG} < 2000 \text{ km s}^{-1}$ (Figure 1), there is a chain of galaxy groups spanning from Virgo [RA=12.5^h, Dec. =+12°] to the Local Void direction [RA=19.0^h, Dec. =+3°]. The kinematics of this structure should be influenced both by galaxies infalling towards the Virgo cluster as well as more eastern galaxies moving away from the expanding Local Void (Nasonova & Karachentsev 2011). This narrow strip of sky crossing the Bootes constellation was decided to be considered in details in the present paper.

2 Observational data on galaxies in the Bootes strip

Based on the Lyon Extragalactic Database = LEDA (<http://leda.univ-lyon1.fr>), we have selected galaxies with radial velocities $V_{LG} \leq 2000 \text{ km s}^{-1}$ relating to the Local Group centroid in the sky region with equatorial coordinates RA = [13.0^h, 18.0^h], Dec. = [−5°, +10°]. Among 2515 extracted objects, 2154 or 86% (!) turned out to be false galaxies, mainly the Milky Way stars. There is also a number of high velocity clouds detected in Arecibo HI survey.

The major part of the considered strip is covered by the optical SDSS survey (Abazajian et al. 2009) as well as HIPASS (Zwan et al. 2003) and ALFALFA (Haynes et al. 2011) HI surveys, which is a certain advantage for our purposes. Using these surveys we performed an independent morphological classification of galaxies and refined the data on their apparent magnitudes and radial velocities. We eliminated several cases when apparent magnitude or radial velocity estimates were attributed to fragments of the same galaxy. New data from the ALFALFA survey gave us an opportunity to determine distances for many galaxies from the Tully & Fisher (1977) relation between luminosity of a galaxy and its HI line width W_{50} (measured at the level of 50% of the peak).

The resulting list of 361 galaxies in Bootes strip obtained by comparing critically the data from different sources and eliminating some ambiguous cases is presented in Table 1. Its columns contain: (1) galaxy number in the known catalogues; (2) equatorial coordinates for 2000.0 epoch; (3) integral apparent magnitude in the B band from the NASA Extragalactic Database (=NED) (<http://ned.ipac.caltech.edu>), LEDA or SDSS; in some cases with discrepant values of B_T from different sources we had reliance on our own eye estimates of the apparent magnitude; (4) galaxy distance (in Mpc) together with the method applied for estimating the distance: “sn” – from Supernova luminosity, “rgb” – from the tip of the red giant branch luminosity, “sbf” – from surface brightness fluctuations (Tonry et al. 2001), “tf” or “TF” – from

the Tully-Fisher relation; in most cases (indicated as TF) distances were estimated by us independently using the relation from Tully et al. (2009):

$$M_B = -7.27(\log W_{50} - 2.5) - 19.00;$$

to correct W_{50} for inclination in the case of dwarf galaxies we assumed their spatial shape to be a spheroid with the axial ratio of 1:2 (Roychowdhury et al. 2013); (5) radial velocity in the Local Group frame and its error (in km s^{-1}); (6) morphological type according to our identification; (7) name of the brightest galaxy in the group (Makarov & Karachentsev 2011) or in the pair (Karachentsev & Makarov 2008) which the considered galaxy belongs to. As it follows from this column data, more than a half (56%) of all galaxies in the Bootes strip form bound systems.

The upper panel of Figure 2 presents the radial velocity distribution of 361 galaxies in the strip. The velocity colorscale is shown under the panel. All the galaxies have radial velocities $V_{LG} > 650 \text{ km s}^{-1}$ except proximate dwarf KKH 86 with $V_{LG} = 209 \text{ km s}^{-1}$ and $D = 2.6 \text{ Mpc}$. Most galaxies with radial velocities lying in the range (700 – 1300 km s^{-1}) are situated on the western side of the strip, neighbouring the Virgo cluster. A circular arc near RA $\simeq 14^h$ marks the zero velocity surface with radius R_0 which separates galaxies falling toward the Virgo centre from those being involved with the cosmological expansion. For the Virgo cluster R_0 value is 7.2 Mpc or 25° (Karachentsev et al. 2014). MK groups (Makarov & Karachentsev 2011) are marked by names of their brightest galaxies. The most notable feature of galaxy distribution in the Bootes strip is the compact group NGC 5846 which numbers 74 members with measured radial velocities (some of them slightly exceed the limit of 2000 km s^{-1} adopted for this research).

The middle panel of Figure 2 represents the morphological type distribution of considered galaxies. Early type galaxies (E, S0, dSph) are plotted as red markers, spirals (Sa–Sdm) as green ones while irregular galaxies (Ir, Im) and blue compact dwarves (BCD) marked with blue. As one can see, most early type galaxies are concentrated among the population of NGC 5846 group and several other groups (NGC 5363, NGC 5638), though certain S0 galaxies (NGC 6010, CGCG 052-15) occur in the general field too.

Among all the 361 galaxies of the Bootes strip, 161 galaxy (45%) have distance estimates. Distance distribution of these galaxies is shown on the lower panel of Figure 2. About 2/3 of them lie in the range of (25±5) Mpc. As most galaxies in the Bootes strip have distances measured from Tully-Fisher relation with an accuracy of $\sim 20\%$, the line-of-sight width of the Bootes filament turns

out to be comparable with the typical distance error. A polyline under the panel represents the running median of D value along right ascension with window of $0^h.5$. As it follows from these data, the major part of the Bootes filament galaxies is located farther than the Virgo cluster which has, according to Mei et al. (2007), the mean distance of 16.5 ± 0.5 Mpc. Going by the running median trend, the Bootes filament seems to be slightly curved and galaxy distances tend to decrease towards the Virgo cluster.

3 The Hubble flow in the Bootes strip

For a galaxy with measured distance, its deviation from the unperturbed Hubble flow can be characterized by an individual Hubble parameter value $H = (V_{LG})/D$ or by a peculiar velocity value $V_{pec} = V_{LG} - H_0 \times D$, where H_0 is fixed to be $72 \text{ km s}^{-1} \text{ Mpc}^{-1}$.

The upper panel of Figure 3 presents individual H value distribution of the Bootes strip galaxies lying in the range from 25 up to $100 \text{ km s}^{-1} \text{ Mpc}^{-1}$. A polyline under the H scale shows the running median drift with window of $0^h.5$ along RA. The most common value is $H = 62 \text{ km s}^{-1} \text{ Mpc}^{-1}$, which remains almost flat from $\text{RA}=13^h.7$ to $17^h.3$. Galaxies in the Virgo infall zone demonstrate clearly a droop of the H median; to the contrary, in the vicinity of the Local Void H value rises which is quite expectable since galaxies move away from the void centre (unfortunately, the galaxy number statistics near the void is poor).

Peculiar velocities distribution of the Bootes strip galaxies is similar (the lower panel of Figure 3). The main body of the Bootes filament is characterized by roughly the same value of $V_{pec} \simeq -250 \text{ km s}^{-1}$ tending to increase near the Local Void boundary and to decrease significantly (to -600 km s^{-1}) near the Virgo cluster.

The relation between radial velocities and distances of galaxies in the Bootes strip is presented in Figure 4, where straight line corresponds to the Hubble parameter value $H_0 = 72 \text{ km s}^{-1} \text{ Mpc}^{-1}$. Galaxies in the Virgo infall zone ($\text{RA} < 14^h.0$) are plotted as open circles while other single galaxies are shown as solid ones. Due to distance errors ($\sim 20\%$), a nonlinear Malmquist bias appears in this Hubble diagram: absolute distance errors for farther galaxies are larger than those for nearer ones, so the whole set of galaxies is shifted rightwards apparently. To reduce Malmquist bias, we use pairs and groups of galaxies with distances measured for two or more members. Mean radial velocities and mean distances for 10 groups and 5 pairs are shown as squares and triangles, respectively, indicating mean distance error bars. Three groups and a

pair in the Virgo infall zone are plotted with open circles. As can be seen, in most cases the deviations of groups and pairs from the general Hubble flow are quite small though exceeding their mean distance errors. The most deviating group beyond the infall zone is NGC 5838 with a peculiar velocity of $\sim 500 \text{ km s}^{-1}$ which is probably due to the influence of the neighbouring massive group NGC 5846.

4 Sub-structures in the Bootes filament

According to the galaxy grouping criterion (Karachentsev & Makarov 2008, Makarov & Karachentsev 2011) the considered region is populated with 13 groups and 11 pairs. Their main properties are presented in Tables 2 and 3, respectively. The columns of Table 2 contain: (1) name of the brightest galaxy in the group; (2) number of group members with measured radial velocities; (3) mean radial velocity in the Local Group frame; (4) group distance (in Mpc) corresponding to the mean distance modulus ($m - M$); (5) dispersion of radial velocities; (6) mean projected harmonic radius of the group; (7) stellar mass logarithm derived from the total luminosity of group members in the K- band; (8) projected mass logarithm (Heisler et al. 1985):

$$M_p = (32/\pi G) \times (N - 3/2)^{-1} \sum_{i=1}^N \Delta V_i^2 \times R_i,$$

where ΔV_i and R_i are radial velocity and projected distance of the i th galaxy relative to the system centre and G is the gravitational constant; (9) projected-to-total stellar mass ratio in logarithmic scale; (10) number of group members with individual distance estimates; (11) the mean-square difference of distance moduli of the group members; in the case $N_D = 1$ we formally put $\sigma(m - M) = 0^m.4$ which corresponds to distance error of 20%.

The data on galaxy pairs are given in Table 3 in the same manner. Here, projected (i.e. orbital) mass is defined as

$$M_p = (16/\pi G) \times \Delta V_{12}^2 \times R_{12},$$

where ΔV_{12} and R_{12} are radial velocity difference and projected separation between the pair components.

a) Galaxy groups.

The most prominent structural unit in the Bootes strip is NGC 5846 group. Being a compact system densely populated with early types galaxies, NGC 5846 group is obviously at the advanced stage of its dynamical evolution. Mulchaey & Zabludoff (1998) mention the presence of X-ray emission around NGC 5846 as the central galaxy of the group. The population of this group was considered by

Zabludoff & Mulchaey (1998), Mahdavi et al. (2005), and Eigenthaler & Zelinger (2010). According to Mahdavi et al. (2005), NGC 5846 group includes about 250 members with absolute magnitudes brighter than $M_R = -12$ mag while the virial mass of the group is $8.4 \times 10^{13} M_\odot$. The same authors noticed the group is significantly isolated along the line of sight: on the 10 sq. deg. area occupied by this group there is not any galaxy lying in the foreground while the nearest neighbouring galaxies in the background appear only at $V_{LG} \geq 6000 \text{ km s}^{-1}$. Based on X-ray emission pattern, Mahdavi et al. (2005) distinguished two subgroups dominated by two elliptical galaxies: NGC 5846 and NGC 5813. Yet, kinematic characteristics distinguish another group, besides NGC 5846 one. This group includes 9 galaxies dominated by S0 type galaxy NGC 5838. The groups around NGC 5846 and NGC 5838 have roughly the same distances: 26.4 Mpc and 25.0 Mpc, but differ significantly in their mean radial velocities: (1803 km s^{-1} and 1269 km s^{-1}). In such a configuration, the total dispersion of radial velocities reaching 320 km s^{-1} (Mahdavi et al. 2005) reduces to 228 km s^{-1} (NGC 5846) and 53 km s^{-1} (NGC 5838) that leads to decrease of the virial mass estimate from $8.4 \times 10^{13} M_\odot$ to $4.8 \times 10^{13} M_\odot$ for the whole complex of galaxies around NGC 5846.

Figure 5 represents a close-up view of galaxy distribution in the region of NGC 5846 group. Another populated group around Sb type galaxy NGC 5746 lies to the west of NGC 5846, as well as a group around E type galaxy NGC 5638, a group around Sab type galaxy NGC 5566 and some more poorly populated groups and pairs. The radii of zero velocity surface for these groups (with virial masses specified in Table 2) are 2.8 Mpc (NGC 5846), 1.0 Mpc (NGC 5838), 2.0 Mpc (NGC 5746) and 1.4 Mpc (NGC 5566). With weighted average distance $D = 26$ Mpc, the angular radii of the infall zones are 6.1° , 2.2° , 4.4° and 3.2° , respectively. Hence, the infall zones around the considered groups overlap substantially and the substructures themselves can merge eventually into a single dynamical system.

It is worth emphasizing that members of the MK-groups (Makarov & Karachentsev, 2011), were found by their radial velocities and projected separations with regard for galaxy stellar masses (K -band luminosities) while their individual distance estimates were not considered. Since most galaxies in the Bootes strip have Tully-Fisher distance estimates with an accuracy of $\sim 20\%$ or 0.4 mag, the scatter of distance moduli estimates inside a group should be ~ 0.4 mag. The data in the last column of Table 2 show that the rms difference $\sigma(m - M)$ weighted by the number of group members N_D is 0.35 mag. Hence, the applied grouping algorithm does not add a substantial number of false members into the groups.

b. Binary galaxies.

The pairs of galaxies from Table 3 are characterized by the median distance of 26 Mpc typical for the whole population of the Bootes strip. The median radial velocity difference for the components of 11 pairs is only 22 km s^{-1} giving evidence for their physical connection. The median projected separation of the components is 180 kpc which is also typical for dynamically bound pairs. The median projected mass of the binary galaxies is $0.8 \times 10^{10} M_\odot$ and the typical projected mass-to-total stellar mass ratio amounts to $M_p/M_* \simeq 7$. For five galaxy pairs having distance estimates for both components, the $(m - M)$ scatter does not exceed the expected tolerance of ~ 0.4 mag.

c. Field galaxies.

As it was noticed afore in this paper, about 44% of galaxies in the Bootes strip are not bound to any system forming the field population. This ratio is just typical for the whole volume of the Local Supercluster, limited by radial velocities $V_{LG} < 3500 \text{ km s}^{-1}$ (Makarov & Karachentsev 2011). Low luminosity objects and late type galaxies are common among the field population. This fact fits well into the paradigm in which masses of galaxies and luminosity of their bulges grow with time due to the repeating hierarchical merging.

As seen from Figure 4, single galaxies in the Bootes strip are more scattered in the Hubble diagram than centres of groups and pairs. This is mainly caused by distance errors. In spite of the distance scatter, single galaxies on the western side of the Bootes strip (open circles) also show the effect of infall towards the Virgo cluster similarly to centers of groups and pairs. It should be noted that distances of some galaxies measured via Tully-Fisher relation differ significantly from those expected from their radial velocities (even taking into account the Virgo-centric infall effect). We have eliminated some of these distance estimates, for example, for dwarf galaxies SDSS 1430+07 and CGCG 75-063 with spurious widths $W_{50} \sim 170 \text{ km s}^{-1}$ attributable to HI flux confusion from neighbouring bright spirals. However, there are some problematic cases in Table 1 with a strong discordance between radial velocities and distances. One of them is an isolated galaxy AGC 238769 with radial velocity of 953 km s^{-1} and distance estimate of 34.0 Mpc. Another case is a flat galaxy FGC 1642 with $V_{LG} = 1168 \text{ km s}^{-1}$ and $D = 34.6$ Mpc, we have excluded from NGC 5248 group members when estimating dispersion of $(m - M)$. Significant deviations of such galaxies in the Hubble diagram not attributable to their wrong HI line width or inclination error can give argument for existent large peculiar motions of these scarce galaxies.

5 Local density of matter in the Bootes strip

The virial (projected) mass distribution of galaxy groups (squares) and pairs (triangles) in the considered strip versus their total stellar mass is depicted in Figure 6. There is a positive correlation between virial and stellar masses, well-known from other data. While masses are small, the significant vertical scatter is caused mainly by projection factors.

According to Jones et al. (2006), the mean density of the stellar matter in the Universe is $4.6 \times 10^8 M_\odot \text{ Mpc}^{-3}$ as $H_0 = 72 \text{ km s}^{-1} \text{ Mpc}^{-1}$. The global matter density $\Omega_m = 0.28$ in the standard Λ CDM model with this Hubble parameter is equivalent to dark-to-stellar matter ratio of $M_{DM}/M_* = 97$. This value is shown as a diagonal in Figure 6. All the groups and all the pairs except one in the Bootes strip are situated under this line. The sum of virial masses-to-sum of stellar masses ratio for all the groups and pairs, $\sum M_p / \sum M_* = 33$, is plotted as a cross. The dashed line drawn through the cross indicates the mean mass density Ω_m (Bootes) $\simeq 0.09$, which is three times smaller than the global cosmic density. Here, we did not consider for contribution of single galaxies, but evidently the field galaxies contribute both to numerator and denominator of the ratio $\sum M_p / \sum M_*$. Moreover, considering them should only reduce slightly this proportion. Thus, the observational data on galaxy motions in the Bootes strip give us an argument that this filamentary structure does not contain a large amount of dark matter at a level of $\Omega_m \simeq 0.28$. This statement refers certainly to virial mass estimates based on internal motions of galaxies in systems. Yet, supposing that 3–5 times larger mass is hidden in the Bootes filament between the groups, then the total mass would be about $4 \times 10^{14} M_\odot$, i.e. comparable with the mass of the Virgo cluster, and the velocity dispersion for centres of groups and pairs should be considerably larger than what is observed.

6 Concluding remarks

Reconstruction the 3D cosmic flow field in the Local Universe undertaken by Courtois et al. (2013) using the Wiener Filter method shows the complex picture of galaxy motions in the region between the Local Void and the Virgo cluster. When the spatial location of the Virgo cluster and the pattern of Virgocentric infall seem to be well-defined, whereas the extent of the Local Void and the position of its centre stay controversial.

In the diagram presented in the Figure 7 we tried to represent position of the Bootes filament relative to the Virgo Cluster and Local Void as two main agents forming

the peculiar velocity field in the Bootes strip. We assumed the distance to the Virgo centre to be 16.5 Mpc (Mei et al. 2007) and the line-of-sight extent of the Local Void to range from 0 to 20 Mpc with the centre lying halfway (Nasonova & Karachentsev 2011). The Local Group with an observer is situated in the lower left corner while the diagram axes roughly correspond to Supergalactic axes SGY and SGZ. This diagram illustrates changing proportions between line-of-sight projected velocities of the Virgocentric infall and of the Void outflow in different regions of the Bootes filament. This sketch allows to understand the behaviour of the mean peculiar velocity (Figure 3) along the filament.

We hope wholesale measurements of galaxy distances both northward and southward of the Bootes strip will give in the near future more detailed information on the Local Void geometry and motions of galaxies in its immediate neighborhood.

Acknowledgments

This work is supported by the Russian Foundation for Basic Research (grant no. 13-02-90407) and the State Fund for Fundamental Researches of Ukraine (grant no. F53.2/15). O.G.Nasonova thanks the non-profit Dmitry Zimin's Dynasty Foundation for the financial support. This research has made use of NASA/IPAC Extragalactic Database (<http://ned.ipac.caltech.edu>) which is operated by the Jet Propulsion Laboratory, California Institute of Technology, under contract with the National Aeronautics and Space administration. We acknowledge the usage of the HyperLeda database (<http://leda.univ-lyon1.fr>) and SDSS archive (<http://www.sdss.org>).

REFERENCES

- Abazajian K.N., Adelman-McCarthy J.K., Agueros M.A., et al. 2009, *ApJS*, 182, 54
- Courtois H.M., Pomarede D., Tully R.B., et al. 2013, *AJ*, 146, 69
- Dietrich J.P., Werner N., Clowe D., et al., 2012, *Nature*, 487, 202
- Eigenthaler P., Zeilinger W.W., 2010, *A&A*, 511, 12
- Haynes M.P., Giovanelli R., Martin A.M., et al. 2011, *AJ*, 142, 170
- Heisler J., Tremaine S., Bahcall J.N., 1985, *ApJ*, 298, 8
- Jones D.H., Peterson B.A., Colless M., Saunders W., 2006, *MNRAS*, 369, 25
- Karachentsev I.D., Tully R.B., E.J.Shaya, et al. 2014, *ApJ*, 782, 4
- Karachentsev I.D., Nasonova O.G., 2013, *MNRAS*, 429, 2677
- Karachentsev I.D., Nasonova O.G., Courtois H.M., 2013, *MNRAS*, 429, 2264
- Karachentsev I.D., 2012, *Astrophys. Bull.*, 67, 115

Karachentsev I.D., Nasonova O.G., Courtois H.M., 2011, ApJ, 743, 123
 Karachentsev I.D., Nasonova O.G., 2010, MNRAS, 405, 1075
 Karachentsev I.D., Kashibadze O.G., Makarov D.I., Tully R.B., 2009, MNRAS, 393, 1265
 Karachentsev I.D., Makarov D.I., 2008, Astrophys. Bulletin, 63, 299
 Karachentsev I.D., Tully R.B., Dolphin A., et al. 2007, AJ, 133, 504
 Karachentsev I.D., Kashibadze O.G., 2006, Ap, 49, 3
 Mahdavi A., Trentham N., Tully R.B., 2005, AJ, 130, 1502
 Makarov D.I., Karachentsev I.D., 2011, MNRAS, 412, 2498
 Mei S., Blakeslee J.P., Cote P., et al. 2007, ApJ, 655, 144
 Mulchaey J.S., Zabludoff A.I., 1998, ApJ, 496, 73
 Nasonova O.G., Karachentsev I.D., 2011, Ap, 54, 1
 Nasonova O.G., de Freitas Pacheco J.A., Karachentsev I.D., 2011, A&A, 532A, 104
 Roychowdhury S., Chengalur J.N., Karachentsev I.D., Kaisina E. I., 2013, MNRAS, 436L, 104
 Sorce J.G., Courtois H.M., Gottloeber S. et al. 2014, MNRAS, 437, 3586
 Spergel D.N. et al. 2007, ApJS, 170, 377
 Tonry J.L., Dressler A., Blakeslee J.P., et al., 2001, ApJ, 546, 681
 Tully R.B., Rizzi L., Shaya E.J., et al. 2009, AJ, 138, 323
 Tully R.B., 1987, ApJ, 321, 280
 Tully R.B., Fisher R.J., 1977, A&A, 54, 661
 Vennik J., 1984, Tartu Astron. Obs. Publ., 73, 1
 Whiting A.B., 2006, AJ, 131, 1996
 Zabludoff A.I., Mulchaey J.S., 1998, ApJ, 496, 39
 Zwaan M.A., Staveley-Smith L., Koribalski B.S. et al., 2003, AJ, 125, 2842

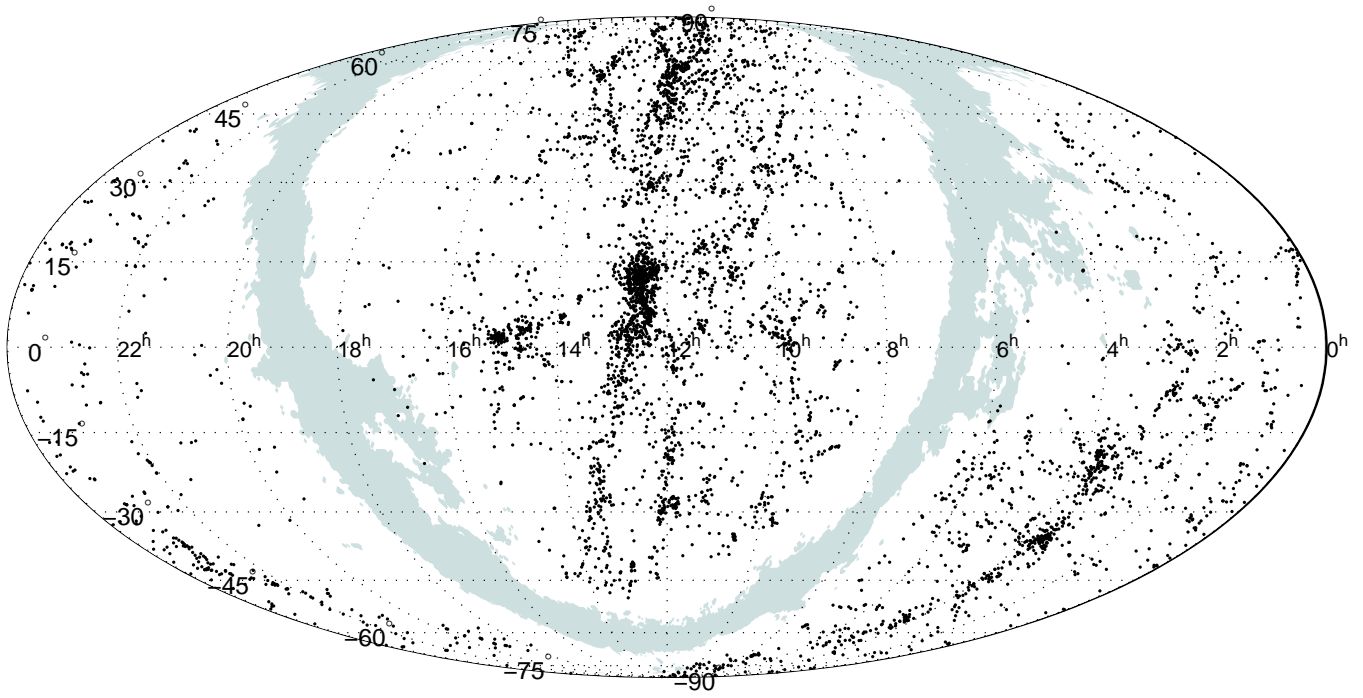


Figure 1: Sky distribution of Local Supercluster galaxies in equatorial coordinates. The region of strong absorption along the Milky Way is filled with gray.

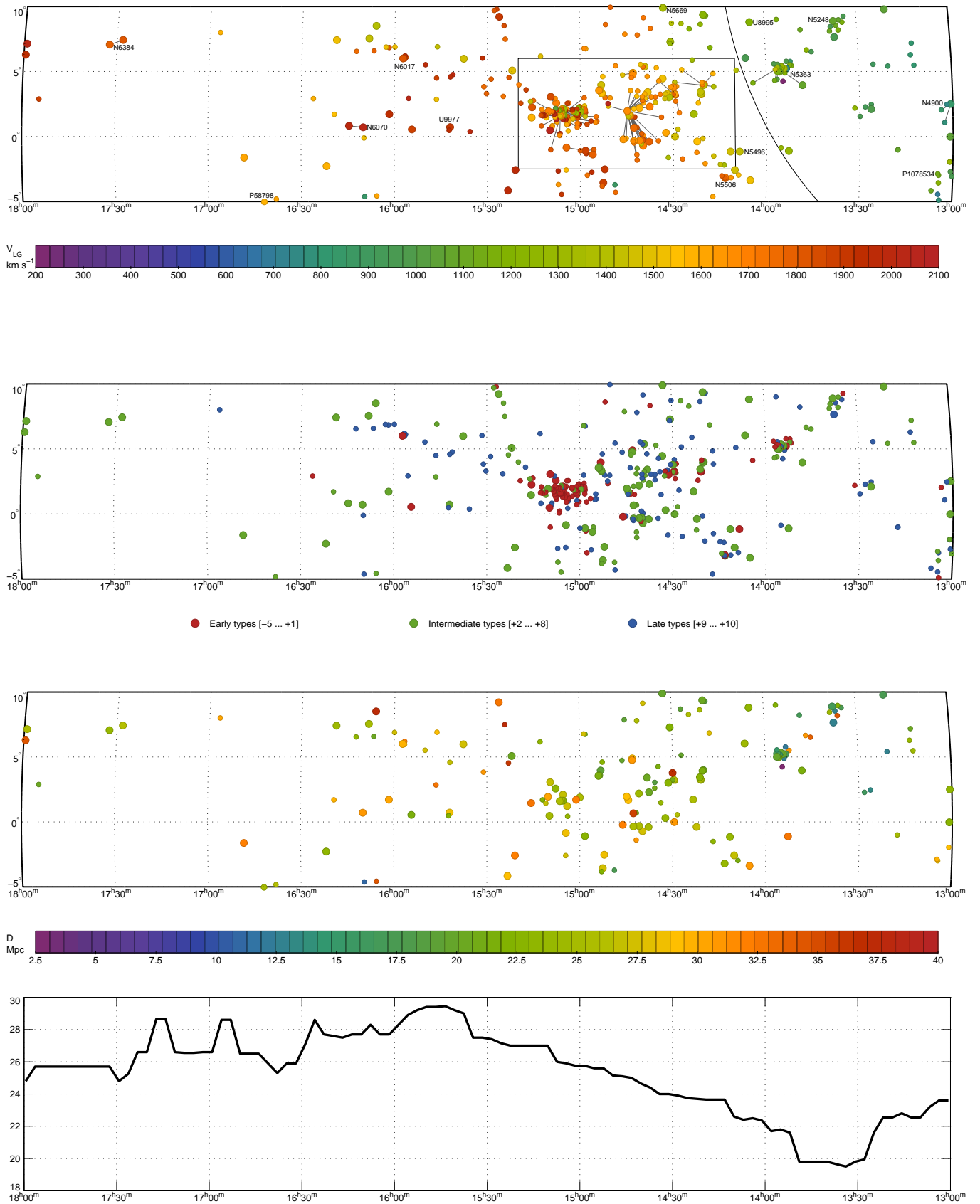


Figure 2: Radial velocity (upper panel), morphological type (middle panel) and distance (lower panel) distributions of galaxies in the Bootes strip. Dwarf galaxies with absolute magnitudes $M_B > -17.0$ are plotted with small circles. A polyline under the lower panel represents the running median of distance with window of $0^{\text{h}}5$.

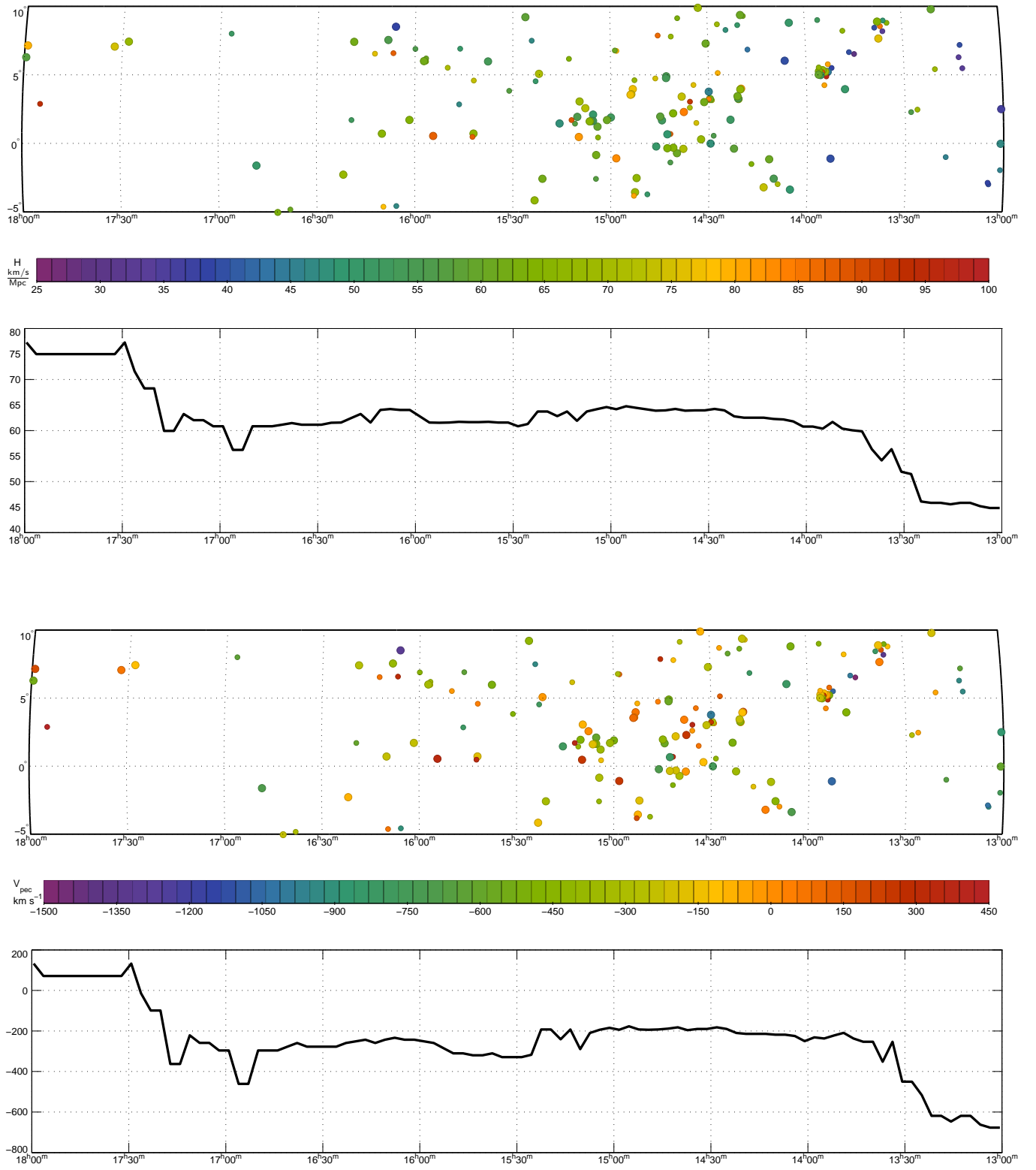


Figure 3: Individual H value (upper panel) and peculiar velocity distributions of galaxies in the Bootes strip. Polygonal lines under the panels correspond to running medians with window of $0^{\text{h}}.5$. Dwarf galaxies are plotted with small circles.

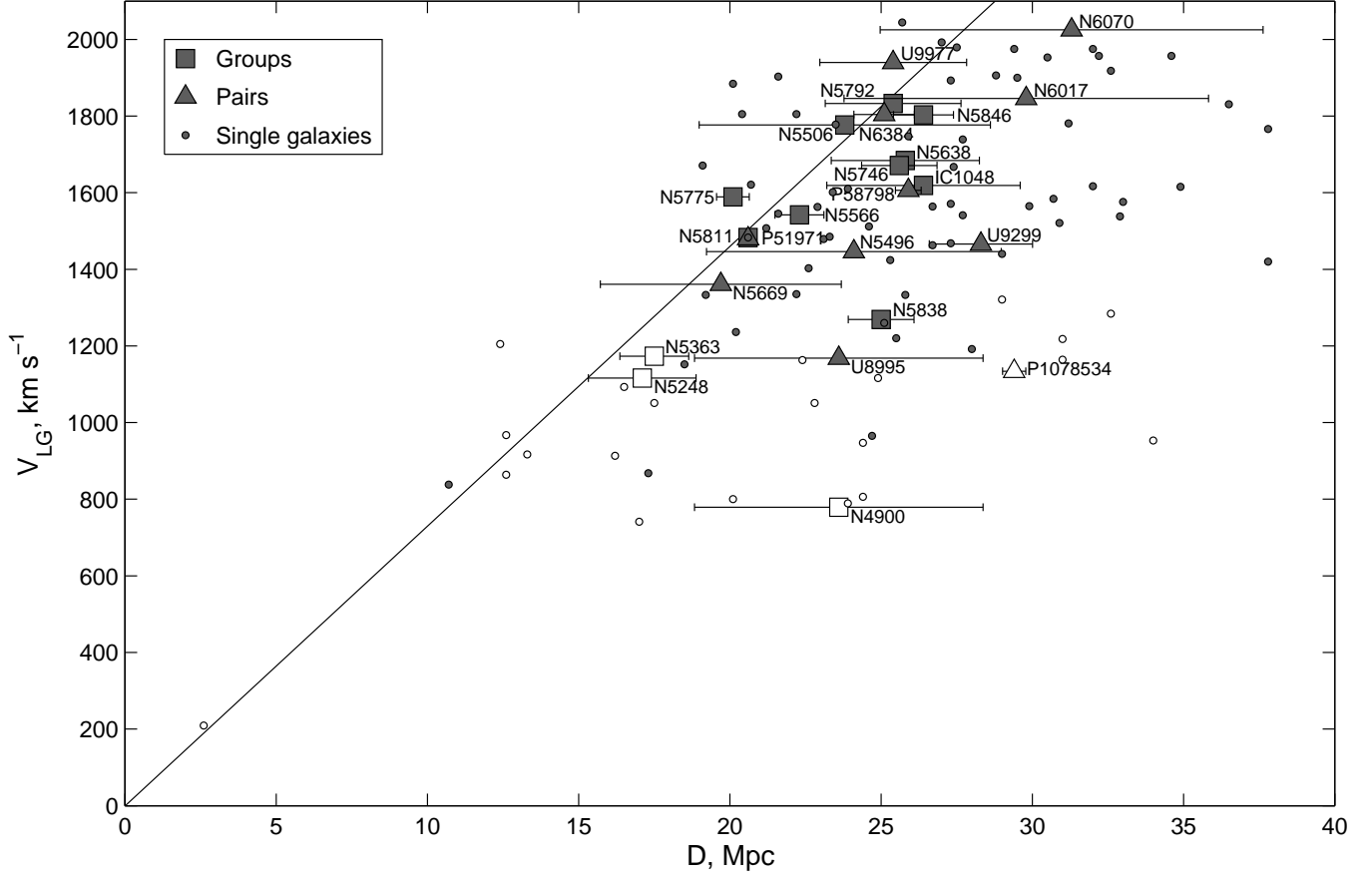


Figure 4: Hubble digram for group centres (squares), pair centres (triangles) and single galaxies (circles). Galaxies and systems in the Virgo infall zone with $RA < 14^h0$ are plotted with open symbols.

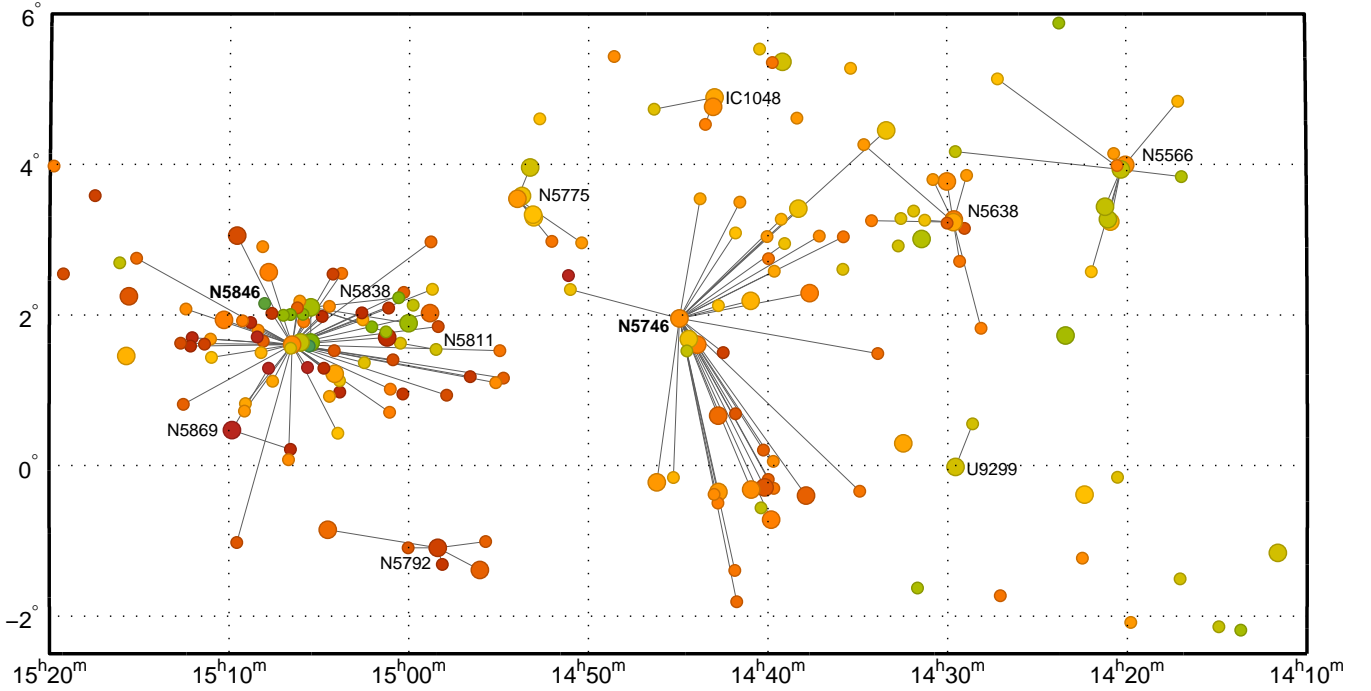


Figure 5: Close-up view of the Bootes strip region containing NGC 5846 and NGC 5746 groups. Members of groups and pairs are linked with their dominating galaxies.

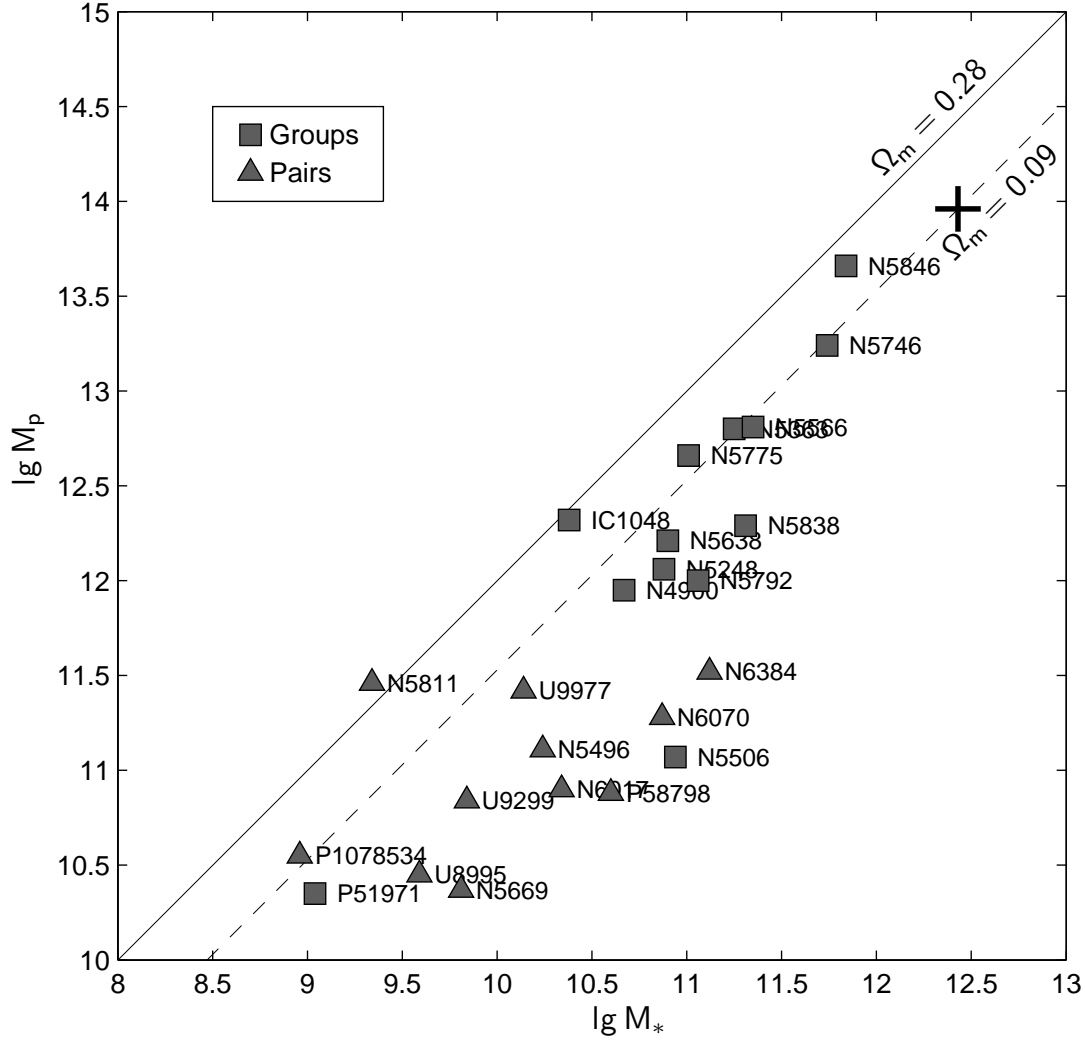


Figure 6: The relation between projected (virial) mass and total stellar mass for galaxy groups (squares) and pairs (triangles). A cross marks virial and stellar mass values for all the Boots strip. Solid and dashed lines indicate the global and the local mean matter density.

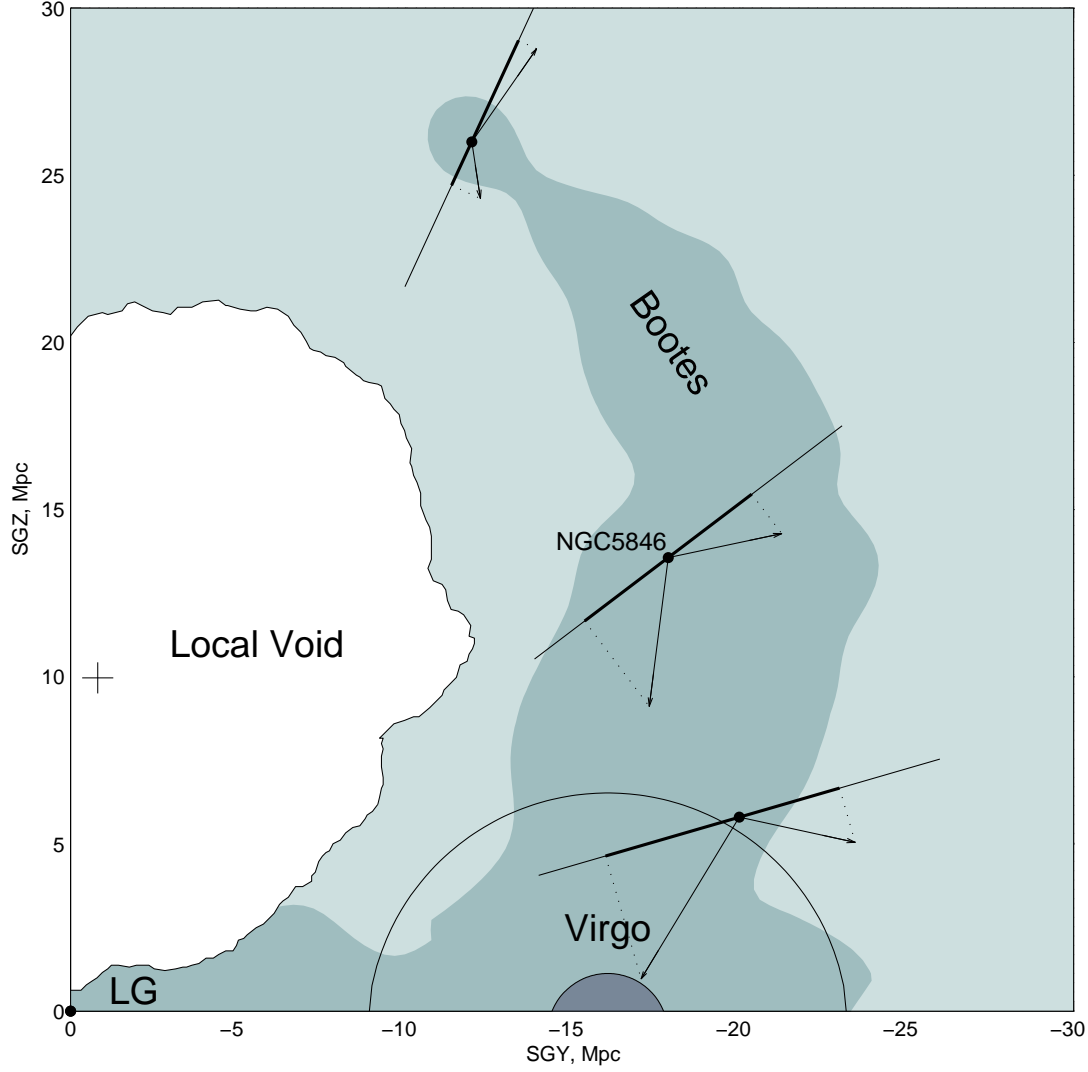


Figure 7: The diagram illustrating the position of the Bootes filament relative to the Virgo cluster and the Local Void. The inner and the outer radii around the Virgo cluster correspond to the virial zone and the zero velocity surface radius R_0 . The projected velocities of the Virgocentric infall and of the Void outflow have different values in different regions of the Bootes filament. An observer (LG) is situated in the lower left corner of the diagram.

Table 1: Galaxies with $V_{LG} < 2000 \text{ km s}^{-1}$ in the Bootes strip: RA = $[13.0, 18.0]^h$, Dec = $[-5, +10]^\circ$

Object	RA (2000.0)	DEC	B_t	D_{Mpc}	V_{LG}	err	T	Group
PGC044733	J130017.5-030359		15.88		963	21	Sm	
NGC4900	J130039.2+023004		11.91	23.6 sn	832	8	Sc	N4900
PGC1084547	J130045.7-024304		18.12		991	89	Ir	
NGC4904	J130058.7-000139		12.67	22.8 tf	1051	8	Sc	
PGC214054	J130100.8-015834		17.39		1216	15	Im	
UGC08127	J130103.7-015712		15.57	29.0 TF	1321	10	Sm	
PGC1227695	J130153.4+022738		17.96		746	8	BCD	N4900
PGC045019	J130240.8+010427		17.47		787	20	BCD	N4900
PGC135818	J130344.2+020224		17.18		844	49	dS0	N4900
PGC170228	J130412.1-045327		14.83		765	64	S0	
UGCA322	J130431.2-033421		14.34		1211	9	Sm	
PGC1078534	J130431.9-025917		16.28	28.8 TF	1148	35	Im	P1078534
PGC3271456	J130436.5-042706		18.93		683	90	Ir	
PGC1080976	J130446.5-025216		16.37	29.8 TF	1113	89	Scd	P1078534
PGC3271328	J130646.8-041021		16.43		1109	64	BCD	
UGC08276	J131206.4+052832		17.12	24.4 TF	806	7	Sm	
UGC08285	J131233.3+071103		15.0	20.1 TF	800	9	Sm	
AGC238737	J131304.4+061707		18.3	23.9 TF	789	21	Im	
PGC046306	J131742.5-010006		15.97	24.9 TF	1116	13	Im	
PGC1128365	J131746.2-010215		16.56		1070	64	Im	
UGC08382	J132032.1+052428		15.22	12.6 TF	864	7	Sm	
UGC08385	J132038.1+094714		14.08	17.5 TF	1051	5	Sm	
AGC238691	J132517.6+053236		17.7		893	15	Ir	
PGC135826	J132615.9+022731		16.80	13.3 TF	917	7	Im	
NGC5147	J132619.6+020603		12.27		978	8	Sm	
KKSG 64	J132812.2+021643		17.44	16.2 TF	913	7	Im	
PGC135828	J132955.7+013239		16.55		939	21	Im	
PGC135829	J133133.9+021115		17.79		1243	89	dE	
SDSSJ13340	J133406.9+091543		17.70		958	39	dE	
KKH 84	J133437.9+084737		15.78	17.6 TF	1156	5	Im	N5248
UGC08575	J133545.6+085809		15.5	22.3 TF	1089	4	Sd	N5248
FGC1642	J133602.4+081108		16.8	34.8 TF	1168	5	Sd	N5248
CGCG73-051	J133643.7+083248		15.88	12.7 TF	1091	5	Ir	N5248
UGC08614	J133726.2+073842		13.21	12.6 TF	967	7	Im	
NGC5248	J133732.1+085306		10.88	16.9 tf	1078	4	Sbc	N5248
UGC08629	J133830.6+082632		15.71	24.4 TF	947	4	Sm	
AGC233601	J133850.8+080629		17.5		1113	5	Sm	
AGC238769	J134506.5+063110		16.9	34.0 TF	953	5	Sdm	
AGC238771	J134641.0+063915		17.11	31.0 TF	1218	47	Sm	
NGC5300	J134816.0+035703		13.06	21.6 tf	1086	8	Sc	N5363
AGC713655	J134822.8+081241		17.8	16.5 TF	1093	20	BCD	
PGC1283560	J135143.0+052647		16.20		1165	24	dE	N5363
SDSSJ13520	J135205.7+054554		17.11		825	5	dS0	
AGC232162	J135210.8+053013		17.5	31.0 TF	1164	33	Sm	
NGC5334	J135254.5-010652		12.97	32.6 tf	1284	7	Sc	
UGC08799	J135319.8+054618		16.32	12.1 sbf	974	28	dE	N5363
NGC5338	J135326.5+051228		13.99	17.0 TF	741	10	S0	
AGC238709	J135353.8+045316		18.0	12.4 TF	1205	14	Ir	
NGC5348	J135411.2+051338		14.18	19.8 tf	1376	7	Sc	N5363
KKH 86	J135433.5+041440		17.08	2.6 rgb	209	5	Ir	
NGC5356	J135458.4+052001		13.63	19.5 tf	1300	7	Sb	N5363
PGC1277985	J135502.7+050525		17.01		1322	7	dEn	N5363
AGC232141	J135504.5+051122		17.18	14.8 TF	1329	5	BCD	N5363

Object	RA (2000.0)	DEC	B_t	D_{Mpc}	V_{LG}	err	T	Group
PGC3303692	J135522.4-005237		18.78		1289	89	BCD	
NGC5360	J135538.7+045906		14.5	21.5 TF	1097	10	Sm	N5363
F721-v2	J135558.0+085947		18.0	22.4 TF	1163	23	Ir	
NGC5363	J135607.3+051517		11.10	16.6 TF	1066	7	S0	N5363
AGC232142	J135609.4+053234		17.38	15.1 TF	1011	8	Ir	N5363
NGC5364	J135612.0+050052		11.19	19.5 tf	1167	6	Sbc	N5363
SDSSJ13562	J135621.3+051944		17.37		1322	68	dE	N5363
UGC08857	J135626.6+042348		15.26		1014	54	Sab	N5363
PGC049602	J135655.6+050907		15.82		1444	25	dEn	N5363
PGC1266441	J135714.1+041826		17.1		1124	30	Sm	N5363
PGC1285591	J135723.6+053427		16.3		984	36	Sph	N5363
UGC08986	J140415.9+040644		15.03		1162	16	dEn	N5363
PGC2807027	J140441.6+084716		18.0		1145	3	Ir	U8995
UGC08995	J140447.3+084803		14.83	23.6 tf	1190	7	Scd	U8995
PGC050229	J140511.1-032211		13.86	30.9 TF	1521	7	Sa	
NGC5470	J140631.7+060144		14.12	24.7 tf	965	10	Sb	
IC0976	J140843.3-010942		14.05		1436	16	S0	N5496
IC0978	J140858.1-025826		15.18	21.6 TF	1545	12	BCD	
AGC242151	J140937.6+050546		16.3		1396	25	Ir	
UGC09057	J141012.9-023433		14.34	26.7 TF	1463	8	Sd	
PGC1075297	J141124.0-031003		18.08		1644	64	BCD	
NGC5496	J141138.1-010938		13.52	24.1 tf	1455	6	Scd	N5496
NGC5506	J141314.9-031227		12.81	23.8 tf	1760	10	Sa	N5506
NGC5507	J141319.9-030856		13.43		1751	18	S0	N5506
PGC1074769	J141324.1-031156		18.35		1786	6	BCD	N5506
KDG 230	J141341.0-021112		17.50		1357	7	Ir	
KKs 65	J141422.2-030156		15.85		1811	6	Sm	N5506
PGC1100661	J141454.2-020823		17.98		1448	6	BCD	
KKR 5	J141657.3+035008		16.91		1409	5	Im	N5566
KKR 6	J141704.2-013020		17.48	23.1 TF	1479	6	Im	
AGC242152	J141707.5+045013		18.13		1582	4	BCD	N5566
PGC1055685	J141710.4-043715		15.69		1623	89	BCD	
AGC243881	J141750.7+065023		17.0	28.0 TF	1200	38	Sm	
AGC244129	J141853.5+091729		17.9	18.5 TF	1152	7	BCD	
UGC09169	J141944.6+092144		14.10	20.2 TF	1236	4	Sm	
PGC3304682	J141948.6-020455		17.23		1650	14	Im	
NGC5560	J142004.9+035931		13.18	20.5 tf	1671	5	Sb	N5566
NGC5566	J142019.9+035600		11.42	21.8 tf	1449	5	Sab	N5566
NGC5569	J142032.1+035859		15.12		1723	5	Scd	N5566
PGC1150546	J142033.9-000918		18.75		1498	89	Ir	
PGC3125420	J142043.5+040837		17.24		1648	44	dE	N5566
AGC714055	J142044.5+083736		16.66	25.1 TF	1260	20	Ir	
NGC5574	J142056.0+031417		13.29	23.9 sbf	1599	10	S0	N5566
NGC5576	J142103.7+031616		11.79	25.5 sbf	1427	17	E	N5566
NGC5577	J142113.1+032609		13.54	23.0 tf	1430	5	Sbc	N5566
PGC1231137	J142200.1+023422		18.19		1568	27	dE	N5566
NGC5584	J142223.8-002315		12.73	26.7 sn	1564	6	Scd	
PGC1123741	J142230.7-011346		17.20		1673	54	Sm	
UGC09215	J142327.2+014334		13.75	25.8 tf	1333	4	Sd	
AGC244252	J142343.7+055237		17.33		1325	7	BCD	
UGC09225	J142424.3+081634		15.4	25.5 TF	1220	4	Sm	
UGC09249	J142659.8+084101		15.01	19.2 tf	1333	3	Sdm	
PGC1111622	J142704.8-014347		18.09		1745	37	BCD	
UGC09252	J142710.8+050801		15.67	19.6 TF	1553	6	Ir	N5566
PGC1206999	J142808.6+014926		18.20		1706	70	Ir	N5638
PGC051719	J142837.8+003311		15.41	26.1 TF	1459	19	Scd	U9299

Object	RA (2000.0)	DEC	B_t	D_{Mpc}	V_{LG}	err	T	Group
SDSSJ14285	J142855.9+035106		18.17		1638	32	dEn	N5638
UGC09285	J142903.9+030856		15.41	25.6 tf	1820	22	Sc	N5638
PGC1235336	J142919.6+024238		17.18		1738	5	dE	N5638
SDSSJ14293	J142933.5+041014		18.29		1448	24	Ir	N5566
UGC09299	J142934.6-000105		14.57	30.8 tf	1473	5	Sd	U9299
NGC5636	J142939.0+031559		13.85		1693	10	S0	N5638
NGC5638	J142940.4+031400		12.16	26.4 sbf	1624	5	E	N5638
UGC09310	J143001.1+031314		15.13	21.2 TF	1794	5	Sm	N5638
IC1022	J143001.8+034622		15.20	37.3 tf	1672	9	Sbc	N5638
SDSSJ14300	J143007.2+084216		18.56		1395	36	Ir	
NGC5645	J143039.4+071630		12.90	22.2 tf	1335	3	Sd	
SDSSJ14304	J143048.2+034750		17.78		1637	24	Ir	N5638
SDSSJ1430	J143048.7+070926		18.09		1288	68	Ir	
PGC1248433	J143116.5+031524		17.04		1536	27	dEn	N5638
IC1024	J143127.1+030030		14.00	22.6 TF	1403	7	S0	
PGC1114278	J143141.2-013729		17.99		1381	20	Ir	
SDSSJ14315	J143153.0+032249		18.53		1491	16	Im	P051971
CGCG75-063	J143220.8+095600		15.57		1373	2	BCD	N5669
UGC9348	J143228.5+001739		14.4	23.9 TF	1610	10	Sb	
PGC1248951	J143235.5+031651		16.80		1490	29	dS0	P051971
NGC5669	J143243.8+095329		12.97	19.7 tf	1349	5	Scd	N5669
PGC051971	J143245.1+025453		15.25		1469	5	Sd	P051971
NGC5668	J143324.3+042701		12.25		1533	3	Scd	N5746
KKSG 66	J143353.5+012912		17.40	23.7 TF	1776	5	Ir	N5746
SDSSJ143414	J143414.3+031502		17.94		1697	58	Ir	N5638
UGC09380	J143439.1+041542		15.15	21.7 tf	1649	7	Im	N5638
PGC1145728	J143454.2-002033		17.29		1734	4	BCD	N5746
UGC09385	J143522.8+051636		16.4		1599	5	Sm	
UGC09392	J143548.5+030218		17.5	18.6 TF	1734	6	Ir	N5746
PGC135851	J143550.1+023619		16.80	21.2 TF	1507	20	Ir	
PGC1344367	J143701.3+081905		17.22		1743	43	En	
PGC052256	J143708.9+030250		16.91		1663	39	Im	N5746
NGC5690	J143741.1+021727		12.48	20.2 tf	1704	5	Sc	N5746
NGC5691	J143753.3-002356		12.90	25.2 TF	1810	9	Sa	N5746
NGC5692	J143818.1+032437		13.46	20.5 TF	1517	24	Sbc	N5746
SDSSJ14382	J143822.6+043648		17.93		1659	4	Ir	
UGC09432	J143904.1+025653		16.06		1529	7	Sm	N5746
NGC5701	J143911.1+052148		12.08		1470	2	Sa	
AGC714204	J143912.4+090806		16.64	27.7 TF	1739	53	Im	
PGC1248765	J143915.5+031621		16.95		1597	37	Sm	N5746
PGC1231422	J143939.3+023455		17.39		1603	37	Sm	N5746
PGC135857	J143940.7-001809		17.31		1749	15	Ir	N5746
PGC1155970	J143942.7+000322		18.21		1685	22	Ir	N5746
AGC241893	J143944.5+052112		17.0		1727	14	Ir	
NGC5705	J143949.8-004306		14.19	27.7 tf	1698	5	Sd	N5746
PGC1236341	J143958.3+024453		17.83		1727	22	Ir	
PGC135858	J143959.9-001110		18.14		1802	3	Ir	N5746
SDSSJ14400	J144002.9+030228		18.54		1635	6	BCD	N5746
NGC5713	J144011.5-001721		12.18		1841	8	Sbc	N5746
PGC1159795	J144015.3+001224		16.93		1806	4	Ir	N5746
PGC1140314	J144023.3-003344		18.24		1438	16	dE	
SDSSJ14402	J144027.6+053155		18.09		1526	30	BCD	
NGC5719	J144056.4-001905		13.27	26.0 tf	1676	5	Sa	N5746
NGC5725	J144058.4+021113		14.56	24.4 TF	1580	7	Scd	N5746
AGC249303	J144119.2+074735		16.1	25.9 TF	1747	2	BCD	
PGC1253386	J144133.7+032948		17.41		1634	4	Sm	N5746

Object	RA (2000.0)	DEC	B_t	D_{Mpc}	V_{LG}	err	T	Group
UGC09469	J144144.3-014827		15.59		1774	7	Sm	N5746
SDSSJ14414	J144148.7+030523		16.34		1549	47	Sm	N5746
UGC09470	J144148.7+004113		15.12	20.7 TF	1834	6	Sd	N5746
UGC09472	J144151.0-012333		15.84	30.9 TF	1737	6	Sdm	N5746
PGC052534	J144229.6+013001		15.21		1876	27	S0	N5746
NGC5733	J144245.9-002104		14.77	25.9 TF	1655	16	Scd	N5746
PGC1216689	J144246.0+020725		16.85		1549	4	Sdm	N5746
UGC09482	J144247.0+003942		15.58	36.1 TF	1782	10	Scd	N5746
PGC1141860	J144247.7-002954		17.79		1718	4	Im	N5746
IC1048	J144258.0+045323		13.95	29.4 tf	1603	6	S0	IC1048
PGC135860	J144300.2-002300		16.61		1688	20	Ir	
UGC09485	J144302.8+044555		15.4	31.3 TF	1672	7	Scd	IC1048
AGC242618	J144329.2+043153		16.65		1710	17	Sdm	IC1048
SDSSJ14434	J144346.9+033234		17.98		1620	4	BCD	N5746
NGC5738	J144356.4+013615		14.77		1700	21	S0	N5746
NGC5740	J144424.4+014047		12.60	29.0 tf	1526	6	Sb	N5746
PGC052652	J144430.9+013122		15.69		1428	20	Im	N5746
NGC5746	J144456.0+015717		11.34	29.0 tf	1680	10	Sb	N5746
PGC1150429	J144515.8-000934		15.74		1598	7	Ir	N5746
UGC09500	J144521.4+075145		16.0	19.1 TF	1671	4	Sm	
NGC5750	J144611.1-001323		12.55	32.4 tf	1635	10	S0a	N5746
AGC242625	J144620.2+044359		17.93	20.0 TF	1491	17	Im	IC1048
AGC245015	J144834.4+052553		17.16		1672	17	Ir	
PGC3277346	J144835.2-041758		17.48		1763	89	Ir	
PGC052893	J144848.0-034259		15.06	17.3 TF	868	6	Sdm	
AGC249197	J144950.7+095630		18.69		1802	40	BCD	
PGC1241857	J145022.9+025729		17.18		1659	3	BCD	N5775
SDSSJ14505	J145059.9+022016		18.56		1516	46	dE	N5746
SDSSJ14510	J145106.8+023127		18.53		2057	21	Im	
PGC1350028	J145132.8+083600		17.68		1758	1	dEn	
SDSSJ14520	J145201.9+025842		17.86		1733	239	BCD	N5775
NGC5768	J145207.9-023147		13.52	28.8 tf	1906	4	Sc	
VV 815	J145234.8-033342		15.14	27.3 TF	1893	5	Sdm	
AGC249264	J145243.3+043617		18.4	22.9 TF	1563	17	Ir	
VV 815	J145254.9-034936		15.12	22.2 TF	1805	30	Sdm	
IC1066	J145302.9+031746		14.27		1546	6	Sb	N5775
IC1067	J145305.2+031954		13.62		1546	6	Sb	N5775
NGC5770	J145315.0+035735		13.18	19.0 sbf	1462	14	S0a	N5775
NGC5774	J145342.5+033457		13.10	20.4 TF	1526	3	Sd	N5775
NGC5775	J145357.6+033239		12.23	21.4 tf	1652	5	Sb	N5775
KKR 14	J145443.0+010943		17.80		1791	7	Ir	N5846
PGC1197564	J145455.8+013132		18.77		1730	18	Ir	N5846
PGC1184577	J145509.3+010602		18.35		1664	5	Ir	N5846
PGC053365	J145542.9-010032		15.78		1802	3	Sm	N5792
UGC09601	J145601.8-012316		14.62		1791	6	Scd	N5792
PGC1083529	J145620.3-024542		18.66		1963	81	Ir	
PGC1186917	J145634.3+011045		17.24		1904	23	dS0	N5846
PGC184824	J145744.8-025913		17.14		1736	55	dEn	
PGC1179522	J145753.1+005603		16.90		1847	16	S0	N5846
PGC184842	J145807.8-011845		16.45		1910	47	S0	N5792
AGC736339	J145808.8+064448		18.23	20.7 TF	1621	15	Ir	
PGC184851	J145821.2+015043		15.99		1858	22	E	N5846
NGC5792	J145822.6-010527		12.12	22.5 tf	1878	5	Sb	N5792
SDSSJ14582	J145828.6+013235		17.64		1461	20	Sph	N5811
CGCG48-085	J145837.8+064630		15.4	27.4 TF	1667	12	Sm	
PGC1223766	J145840.9+022024		18.36		1515	21	dEn	N5846

Object	RA (2000.0)	DEC	B_t	D_{Mpc}	V_{LG}	err	T	Group
PGC1242097	J145846.1+025808		16.39		1776	49	BCD	N5846
PGC053521	J145848.7+020125		14.87		1779	12	E	N5846
SDSSJ14594	J145944.8+020752		18.39		1432	59	Sph	
NGC5806	J150000.4+015329		12.35	25.6 tf	1328	5	Sb	N5838
PGC053577	J150001.3-010528		15.81		1842	3	BCD	N5792
PGC053587	J150016.6+021802		15.50		1800	17	SO	N5846
SDSSJ15001	J150019.2+005700		17.56		1927	2	Sph	
NGC5811	J150027.0+013725		14.76		1498	16	Sm	N5811
SDSSJ15003	J150033.0+021349		17.24		1237	36	Sph	N5838
PGC1193898	J150052.6+012418		16.87		1868	34	dEn	N5846
SDSSJ15010	J150100.9+010050		18.03		1716	21	Ir	N5846
MRK 1390	J150103.1+004227		15.88		1722	15	dS0	N5846
SDSSJ15010	J150107.0+020525		18.33		1921	26	Sph	N5846
NGC5813	J150111.3+014207		11.52	32.1 sbf	1942	6	E	N5846
PGC1205406	J150115.9+014625		18.06		1345	44	dE	N5838
UGC09661	J150203.5+015028		14.81		1213	5	Sdm	N5838
PGC1192611	J150228.2+012151		18.49		1500	44	Sph	N5846
SDSSJ15023	J150233.0+015609		18.18		1619	60	Sph	N5846
SDSSJ15023	J150236.0+020139		18.11		1946	29	dE	N5846
PGC1230503	J150344.2+023309		17.56		1743	27	dE	N5846
SDSSJ15034	J150349.9+005835		16.99		1971	80	Im	
PGC1185375	J150350.3+010737		16.48		1539	19	dE	N5846
KKR 15	J150356.2+002546		17.32	23.7 TF	1555	6	BCD	N5846
NGC5831	J150407.0+011312		12.44	27.5 sbf	1626	5	E	N5846
PGC1197513	J150408.4+013128		16.43		1816	17	S0a	N5846
PGC1230189	J150413.1+023235		15.89		1887	22	E	N5846
PGC1179083	J150423.8+005506		18.12		1626	2	dE	
PGC1216386	J150424.7+020653		17.44		1674	23	dE	N5846
UGC09682	J150430.2-005105		14.9	28.7 TF	1777	7	Sm	N5792
KKR 16	J150434.2-023513		16.51	27.3 TF	1571	4	Ir	
PGC1190315	J150442.9+011727		16.96		1944	24	dE	N5846
SDSSJ15044	J150448.5+015851		18.07		1937	23	Sph	N5846
NGC5838	J150526.3+020558		11.79	27.0 tf	1334	10	S0	N5838
NGC5839	J150527.5+013805		13.69	22.6 sbf	1198	15	S0	N5838
PGC1199471	J150531.8+013516		18.15		947	35	dEn	
PGC1190714	J150537.7+011811		17.43		2058	22	dEn	N5846
PGC1209872	J150550.5+015430		16.93		1701	26	dE	N5846
PGC1213020	J150553.2+020028		18.35		1266	20	Ir	N5838
PGC3092767	J150559.5-042741		16.32		1916	45	Sa	
NGC5845	J150600.8+013802		13.44	25.9 sbf	1424	10	E	N5846
PGC1218738	J150603.4+021106		16.34		1648	23	Sm	N5846
PGC1215798	J150611.3+020545		17.64		1787	3	Sd	N5846
NGC5846	J150629.2+013623		11.09	25.6 sbf	1688	5	E	N5846
SDSSJ15063	J150634.2+001256		17.87		1979	90	dEn	N5869
PGC3119319	J150634.2+013332		16.13		1488	24	E	N5846
NGC5841	J150635.0+020018		14.55		1220	15	S0	N5838
PGC1156476	J150641.0+000436		18.07		1678	30	dE	N5846
SDSSJ15065	J150658.3+015940		17.8		1283	1	Sph	N5838
PGC1067957	J150704.8-034201		16.39		1638	45	Sm	
PGC1085904	J150708.1-023946		17.92		1992	4	Im	
PGC1185172	J150734.2+010714		17.64		1606	37	dE	N5846
PGC054004	J150737.2+020110		15.86		1907	30	dEn	N5846
NGC5854	J150747.7+023407		12.65	23.5 TF	1716	8	S0	N5846
PGC054016	J150747.8+011732		15.67		2073	24	dEn	N5869
PGC1217593	J150801.4+020904		18.04		1048	20	dE	
PGC054037	J150805.6+013906		16.08		1813	20	Sa	N5846

Object	RA (2000.0)	DEC	B_t	D_{Mpc}	V_{LG}	err	T	Group
NGC5846:[M	J150808.5+025418		18.2		1663	1	Ir	
SDSSJ15081	J150812.4+012959		18.02		1579	35	Sph	N5846
PGC1206166	J150822.7+014755		18.08		1668	39	Sph	N5846
NGC5846:[M	J150825.6+014225		18.9		2025	1	Sph	
PGC1209573	J150847.2+015400		16.67		1989	21	dE	N5846
PGC1176385	J150904.3+004919		16.81		1616	3	Im	N5846
SDSSJ15090	J150907.9+004329		17.69		1642	23	Ir	N5846
PGC1210284	J150914.9+015517		16.64		1717	17	dE	N5846
PGC1128787	J150933.6-010118		17.56		1820	4	En	N5846
NGC5864	J150933.6+030310		12.70	27.0 tf	1868	4	S0	N5846
NGC5869	J150949.4+002812		13.15	24.9 sbf	2058	4	E	N5869
UGC09746	J151016.8+015601		14.84	30.4 TF	1714	6	Sbc	N5846
UGC09751	J151058.5+012615		15.62	27.0 TF	1551	15	Scd	N5846
PGC1202458	J151101.3+014050		17.28		1653	23	dE	N5846
SDSSJ15112	J151121.5+013639		17.8		1900	76	Sph	
UGC09760	J151202.5+014155		15.20	22.4 TF	2003	2	Sd	N5846
PGC1199418	J151208.2+013509		17.00		1937	17	En	N5846
PGC1215336	J151224.0+020448		16.94		1675	24	dEn	N5846
PGC1176138	J151231.7+004845		16.32		1806	60	Ir	N5846
PGC1200646	J151241.4+013724		17.25		1863	36	dE	N5846
AGC258278	J151245.0+060951		18.2	23.3 TF	1485	22	Im	
PGC1236445	J151509.4+024507		16.89		1757	21	dS0	N5846
PGC054452	J151534.6+021454		14.82		1834	22	S0	
UGC09787	J151542.8+012721		15.40	33.0 TF	1576	10	Scd	
PGC1234821	J151606.0+024131		17.23		1448	1	Sd	
PGC3124577	J151729.4+033508		17.36		1892	19	BCD	
PGC1230249	J151913.4+023242		16.17		1873	1	S0	
AGC252596	J151947.9+035841		17.7		1708	56	Scd	
NGC5913	J152055.4-023441		14.02	32.0 tf	1975	11	Sa	
NGC5921	J152156.5+050413		11.68	20.6 sn	1483	1	Sbc	
UGC09830	J152300.8+043145		15.91	36.5 tf	1831	5	Sc	
PGC054944	J152320.1-040906		13.51	29.4 tf	1975	6	Sab	
AGC258405	J152411.4+072918		17.25	37.8 TF	1766	1	Sd	
AGC258127	J152432.9+083056		17.4		1865	42	Sm	
PGC3123131	J152450.1+030453		17.58		1744	2	BCD	
UGC09845	J152605.5+091215		15.43	32.6 tf	1918	2	Sbc	
SDSSJ15265	J152655.4+094657		18.23		1884	71	Sph	
AGC251585	J152744.5+094157		16.93		1840	20	Sm	
SDSSJ15284	J152845.0+042421		17.16		1793	0	BCD	
PGC3123706	J153016.7+031722		17.62		1798	3	BCD	
KKR 20	J153106.1+034947		16.50	31.2 TF	1781	2	Ir	
SDSSJ15313	J153133.3+060131		18.25		1947	1	Im	
PGC1164369	J153536.1+002231		17.68		2022	4	Im	
NGC5964	J153736.2+055825		13.42	27.3 tf	1468	2	Sd	
AGC258331	J154106.3+044510		18.04		1996	8	Im	
AGC258332	J154156.9+043448		18.0	27.0 TF	1992	26	Ir	
UGC09977	J154159.6+004246		14.61	28.9 tf	1918	3	Sbc	U9977
UGC09979	J154219.4+002829		14.94	22.4 TF	1963	3	Ir	U9977
UGC10023	J154609.7+065354		15.66	29.0 TF	1440	5	Sm	
UGC10025	J154624.3+025039		16.88	32.9 TF	1538	2	Sd	
SDSSJ15462	J154624.6+042921		18.37		1879	1	BCD	
AGC258343	J154958.0+053102		18.44	27.5 TF	1979	29	Ir	
NGC6010	J155419.2+003235		13.14	21.6 tf	1903	11	S0	
SDSSJ15552	J155522.4+025515		18.90		2040	21	Ir	
SDSSJ15561	J155614.4+060553		17.6		1857	46	Ir	N6017
AGC252891	J155636.8+061139		16.99	32.2 TF	1957	5	Ir	

Object	RA (2000.0)	DEC	B_t	D_{Mpc}	V_{LG}	err	T	Group
AGC258349	J155637.0+055807		17.5	29.5 TF	1900	37	Ir	
NGC6017	J155715.4+055954		13.80	29.8 sbf	1835	8	S0	N6017
AGC258430	J155955.5+065303		18.12	27.7 TF	1541	20	Ir	
IC1158	J160134.1+014228		13.3	30.5 tf	1953	6	Sc	
AGC716496	J160148.4+065018		17.9		1820	3	Ir	
SDSSJ16024	J160247.9+065231		18.0		1516	3	BCD	
KKSG 48	J160540.8-043419		17.5	34.9 TF	1615	1	Sm	
CGCG079-46	J160602.1+083024		15.8	37.8 TF	1420	14	Sm	
CGCG051-43	J160641.0+063451		15.2	20.4 TF	1805	24	Im	
IC1197	J160817.2+073218		14.1	25.3 tf	1424	4	Sd	
PGC057323	J160936.8-043716		15.5	10.7 tf	838	6	Im	
UGC10229	J160943.9-000655		16.6		1522	5	Im	
NGC6070	J160958.7+004234		12.45	31.3 tf	2033	6	Scd	N6070
AGC268216	J161220.5+063237		17.7	23.5 TF	1778	23	Ir	
UGC10290	J161433.0+004918		15.2		2017	4	Sm	N6070
NGC6106	J161847.1+072436		12.84	24.6 tf	1512	7	Sc	
CGCG024-01	J161918.2+014211		15.4	29.9 TF	1565	7	Sm	
NGC6118	J162148.6-021700		11.0	23.4 tf	1601	2	Sc	
CGCG052-15	J162604.3+025424		15.2		1599	32	S0	
PGC058661	J163808.6-044918		15.5	26.5 tf	1612	5	Sd	P58798
PGC058798	J164203.1-050157		14.87	25.3 tf	1600	2	Sbc	P58798
UGC10554	J164821.3-013708		14.90	32.0 TF	1617	9	Scd	
KKR 30	J165638.5+075955		17.0	30.7 TF	1584	6	Ir	
UGC10862	J172809.0+072521		14.4	26.6 TF	1816	8	Sc	N6384
NGC6384	J173224.2+070337		11.14	23.9 tf	1792	8	Sbc	N6384
UGC11030	J175434.2+025251		14.9	20.1 TF	1884	9	Sc	
UGC11074	J175907.4+070829		13.9	25.7 tf	2044	9	Scd	
NGC6509	J175925.3+061713		13.1	34.6 TF	1957	9	Sc	

Table 2: Groups in the Bootes strip

Group	N_v	$< V_{LG} >$	D	σ_v	R_h	$\log M_*$	$\log M_p$	$\log M_p/M_*$	N_D	$\sigma(m - M)$
		km/s	Mpc	km/s	kpc	M_\odot	M_\odot			
N4900	8	779	23.6	36	116	10.67	11.95	1.28	1	(0.4)
N5248	5	1116	17.1	38	151	10.88	12.06	1.18	4	0.43
N5363	17	1173	17.5	144	165	11.25	12.80	1.55	9	0.41
N5506	4	1777	23.8	23	35	10.94	11.07	0.13	1	(0.4)
N5566	12	1542	22.3	103	196	11.35	12.81	1.46	6	0.19
N5638	12	1684	25.8	74	203	10.90	12.21	1.31	5	0.44
P51971	3	1483	20.6	10	100	9.04	10.35	1.31	0	-
IC1048	4	1619	26.4	83	150	10.38	12.32	1.94	3	0.43
N5746	38	1671	25.6	107	296	11.74	13.24	1.50	15	0.40
N5775	7	1589	20.1	87	120	11.01	12.66	1.65	3	0.10
N5792	6	1833	25.4	48	290	11.06	12.00	0.94	2	0.26
N5838	9	1269	25.0	53	210	11.31	12.29	0.98	3	0.16
N5846	74	1803	26.4	228	415	11.84	13.66	1.82	9	0.24

Table 3: Pairs in the Bootes strip

Name	$\langle V_{LG} \rangle$	ΔV_{12}	D	R_{12}	$\log M_*$	M_p	$\log M_p/M_*$	N_D	$\sigma(m - M)$
	km/s	km/s	Mpc	kpc	M_\odot	M_\odot			mag
P1078534	1134	21 ± 9	29.4	68	8.96	10.55	1.59	2	0.04
P1080976									
U8995	1168	45 ± 8	23.6	12	9.59	10.45	0.86	1	(0.4)
P2807027									
N5496	1446	19 ± 17	24.1	305	10.24	11.11	0.85	1	(0.4)
IC976									
U9299	1466	14 ± 20	28.3	304	9.84	10.84	1.00	2	0.18
P051719									
N5669	1361	24 ± 6	19.7	35	9.81	10.37	0.56	1	(0.4)
CGCG75-63									
N5811	1480	37 ± 26	20.6	180	9.34	11.46	2.12	-	-
SDSS14582									
U9977	1940	45 ± 4	25.4	111	10.14	11.42	1.28	2	0.28
U9979									
N6017	1846	22 ± 47	29.8	141	10.34	10.90	0.56	1	(0.4)
SDSS15561									
N6070	2025	16 ± 7	31.3	628	10.87	11.28	0.41	1	(0.4)
U10290									
P58798	1606	12 ± 6	25.9	450	10.60	10.88	0.28	2	0.05
P58661									
N6384	1804	24 ± 11	25.1	488	11.12	11.52	0.40	2	0.12
U10862									